IOWA STATE UNIVERSITY
Digital Repository

2009

Heat Transfer Enhancement in Thermoelectric Power Generation

Shih-yung Hu
Iowa State University

Heat transfer enhancement in thermoelectric power generation

by

"Kenny" Shih-Yung Hu

A thesis submitted to the graduate faculty

in partial fulfillment of the requirements for the degree of

MASTER OF SCIENCE

Major: Aerospace Engineering

Program of Study Committee:

Tom I-P. Shih, Major Professor

Z.J. Wang

Fred Haan

Iowa State University

Ames, Iowa

2009

TABLE OF CONTENTS

iii

LIST OF FIGURES

LIST OF TABLES

ACKNOWLEDGEMENTS

ABSTRACT

Heat transfer plays an important role in thermoelectric (TE) power generation because the higher the heat-transfer rate from the hot to the cold side of the TE material, the higher is the generation of electric power. However, high heat-transfer rate is difficult to achieve compactly when the hot and/or the cold sources are maintained by a flow of gas such as waste heat from the gas exhaust of an engine or a power plant. Also, when the temperature of the hot and the cold sources differs considerably, thermal stress can create damage and thereby affect reliability and service life.

In this study, computational fluid dynamics (CFD) analyses were performed to evaluate two compact gas-phase heat exchangers (HXs) on their ability to enable high heat-transfer rates from the hot to the cold sides of the TE material with minimal thermal stress. One HX utilizes the leading portion of developing momentum and thermal boundary layers, and the other HX involves jet impingement. The CFD analyses take into account the convection heat transfer of the hot gas in the HX flow passages and the conduction heat transfer in the HX walls, the TE materials, the electrical conducting plates, and the insulation material that fills the space between the TE material, the conducting plates, and the HX walls. Both laminar and turbulent flows in the HX flow passages were investigated. When the flow is turbulent, the analysis of the gas phase is based on the ensemble-averaged continuity, Navier-Stokes, and energy equations, closed by the realizable k-ε turbulence model that are integrated to the wall (i.e., wall functions were not used). The analysis of the solid phase is based on the Fourier law.

Results obtained show the two HX designs studied to be useful in increasing heat-transfer rate through the TE material with minimal thermal stresses. For the HX that utilizes the leading part of the boundary-layer flow, a heat-transfer rate of 1 W/cm2 could be achieved with reasonable pressure loss. For the HX with jet impingement, a heat-transfer rate of about 3 W/cm2 could be achieved but the pressure loss is considerably higher.

CHAPTER I. Introduction

Thermoelectric materials (TE) are semiconductors that can directly convert between the flow of thermal energy and the flow of electrical energy.[1,2] When a temperature difference is imposed across the TE material, electrical energy is generated. When an electrical potential is imposed across the TE material, a temperature gradient is created that acts as refrigeration. The primary advantage of TE power generation or refrigeration is that there are no moving parts. Applications of this technology include recovering energy from waste heat in the exhaust gas of engines and power plants, powering satellite systems in space, and providing thermal management.

Figure 1 shows a typical TE couple, the most basic unit for TE energy conversion, and a heat exchanger with embedded TE couples for TE power generation.
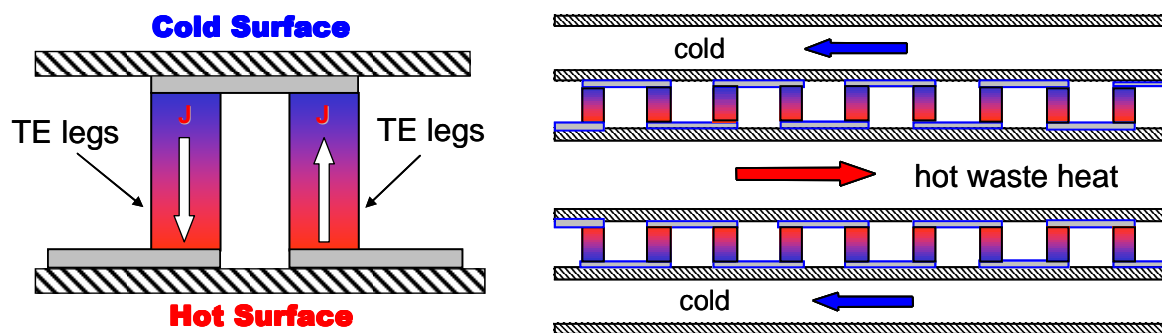
Fig. 1. Left: TE couple (direction of electric current flow in TE legs marked by white arrows; solid gray denotes conducting plates; striped denotes HX walls). Right: heat exchanger with embedded TE couples.

There are three main issues in TE power generation. The first is how to create TE materials with high conversion efficiency (i.e., the fraction of heat transferred that is converted to electrical energy). Z is a figure of merit on conversion efficiency. Its definition is

$$ZT = \frac{\sigma S^2}{\lambda} \frac{T_h + T_c}{2}$$

where σ is the electrical conductivity; λ is the thermal conductivity; S is the Seebeck coefficient; and T_h and T_c are the hot and cold temperatures imposed on the TE device. The best of the current TE materials has values of ZT near unity. If ZT can exceed two in the temperature ranges of interest, then the efficiency of TE devices become highly competitive with other engines. The second main issue is how to maximize the heat-transfer rate across the hot and cold sides of the TE materials because the higher the heat-transfer rate, the higher is the electric current generated. High heat-transfer rate is difficult to accomplish compactly when the hot and/or the cold sides are maintained by flow of gases, where heat-transfer coefficients are orders of magnitude lower than those associated with liquid or two-phase flow. The third issue is how to minimize thermal stresses and the damages that can result when the TE device must operate across large temperature differences with considerable thermal expansion/contraction.

A number of investigators have studied heat-transfer (HT) issues in TE devices. These studies can be divided into three categories – HT analysis of the TE couples, HT analysis of HXs, and HT analysis of TE couples embedded in HXs. HT in TE couples (see Fig. 1) in

turn can be classified as those that address micro- and nano-scale couples and those that address macro-scale couples. For micro- and the nano-scale TE couples, transient analysis based on ballistics-diffusive equations are needed to account for phonon effects.[3-5] Bhandari[6] provides an excellent overview on lattice thermal transport along with electronic thermal transport in heavily doped TE material. For larger couples (e.g., couples with mm or bigger sized TE legs), the HT in TE couples has typically been modeled as one dimensional from the hot to the cold sides[1,7] Hogan & Shih[8] and Harris, et al.[9] developed a mathematical model and computer program to study the three-dimensional heat transfer and electric current flow in a TE couple with and without insulation material between the TE legs. Zhu, et al.[10] studied the natural convection and the radiation heat transfer in the region between the TE legs with a temperature difference of 600K over 1 cm. On HT analysis of HXs, there is a large body of literature though not necessarily applied to thermoelectric power generation. These include the extensive literature on internal cooling of gas-turbine components.[11-13] From the literature, it is well known that HT is highest when the thermal boundary-layer is the thinnest. Thus, the leading portion of boundary layers in short ducts and jet impingement are leading candidates for compact HXs.[11-16] On HT analysis of thermoelectric power generators (TEPG) that has TE couples embedded in HXs, little has been reported except those based on one-dimensional analysis.[1,2]

The objective of this study is twofold. First, analyze the three-dimensional flow and heat transfer in a thermoelectric power generator (TEPG) with the HX and its embedded TE couples. Second, examine two compact gas-phase heat-exchanger (HX) designs on their ability to enable high heat-transfer rates from the hot to the cold sides of the TE material with

minimum thermal stress. This study will be accomplished by using computational fluid dynamics (CFD) analyses that account for the heat-transfer processes in the gas phase and in the solid phases.

The remainder of this paper is organized as follows. First, design concepts that can minimize thermal stresses are explained. Afterwards, the two TEPGs with compact HXs are described. This is followed by the formation of problem, numerical method of solution, results generated, and summary.

CHAPTER II. Design Concept to Minimize Thermal Stresses

In traditional designs, TE couples are sandwiched between the hot and the cold plates as shown on the left in Figs. 1 and 2. With such a design, there is no room for thermal expansion/contraction of the TE legs as operating temperature changes. One way to resolve this problem is to allow the walls that connect the hot and cold plates to be flexible or stretchable but need to maintain structural integrity of the overall device. Shown on the right in Fig. 2 is a design with rigid walls that connect the hot and cold plates but allow for thermal expansion/contraction. This is accomplished by cutting holes into the hot plate to allow the TE legs of the TE couple to expand and contract freely through the holes as temperature changes. With such a design, the TE legs are structurally coupled only to the cold plate but thermally coupled to the hot and the cold sides. To maintain the structural integrity of TE legs from erosion, the portion of the TE legs exposed to the hot gases could be coated. This TE couple design will be utilized in this study.
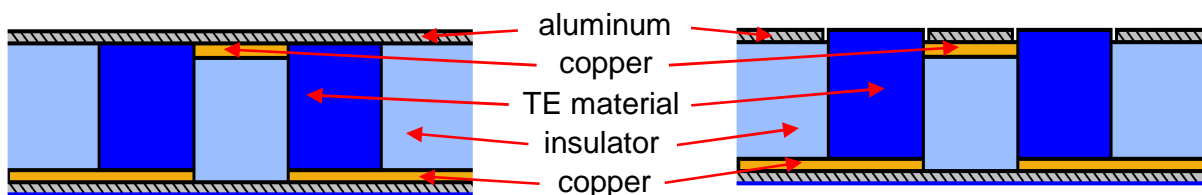
Fig. 2. Left: traditional design (TE couple sandwiched by the hot and cold surfaces (Al plates). Right: new design (TE legs of TE couple structurally disconnected from the hot side but connected thermally).

CHAPTER III. Description of Problem

In this study, two compact heat-exchanger (HX) designs for thermoelectric power generators (TEPG) are examined on their ability to enable high heat-transfer rates from the hot to the cold sides of the TE material in which the design concept illustrated on the left of Fig. 2 is utilized. One HX utilizes the leading portion of a developing thermal boundary layer (Fig. 3), and the other HX involves jet impingement (Fig. 4). The details of each of these two HX designs with embedded TE couples are described below.
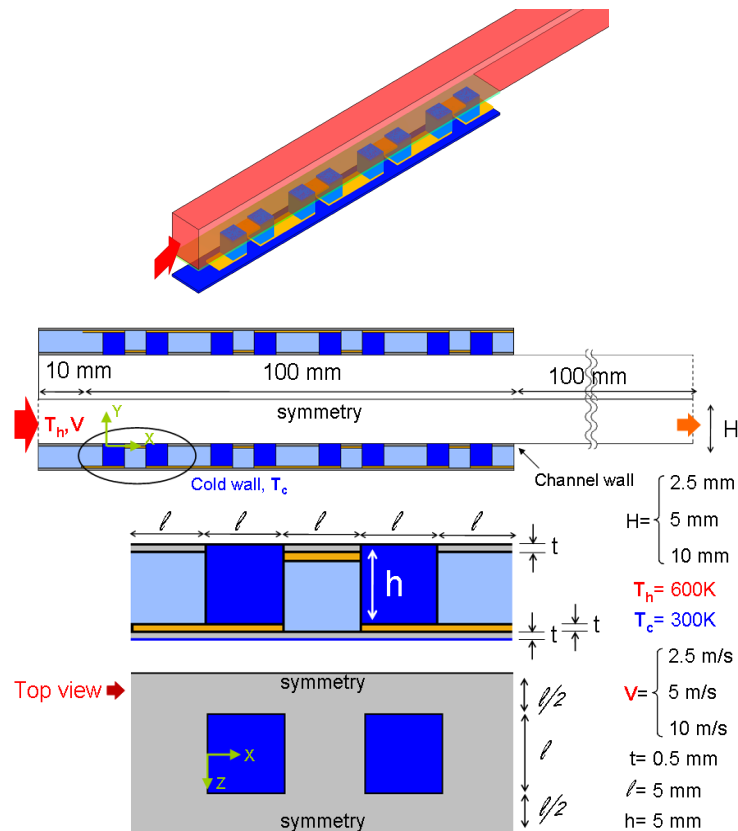
Fig. 3. Schematic of TEPG involving a developing thermal boundary layer.

Fig. 4. Schematic of TEPG involving impinging jets.

TEPG 1 (developing thermal boundary) The TEPG problem shown in Fig. 3 consists of a 210 mm long channel made up of four parallel plates. The middle two plates are separated by 2H in which three values of H were investigated (H can be 2.5, 5, or 10 mm). Hot air enters the middle two plates at X = -15 mm with a uniform temperature T_h of 600 K and a uniform velocity V along the X direction; three values of V were investigated (V can be 2.5 m/s, 5 m/s, or 10 m/s). The back pressure at the exit of this hot-gas passage at X = 200 mm is maintained at 1 atm. For the two outer pairs of plates, each pair sandwiches four rows of TE couples (row is along Z direction). The temperature of the outer wall of the two outer most plates (at Y = -(h+2t) and Y = 2H+(h+2t)) is maintained at T_c of 300K. All plates of

the channel have thickness t of 0.5 mm and are made of aluminum with thermal conductivity k of 202.4 W/m-K. The four rows of TE couples are located at X = 0, 25 mm, 50 mm, and 75 mm and are spaced by 5 mm in the spanwise (X direction) direction. Each TE couple has two TE legs (one p- and one n-type TE material) with 5 x 5 mm^2 cross section and a height of 5 mm that are connected by copper plate with thickness t of 0.5 mm. The TE couples in the same row are separated by 0.5 mm in the spanwise direction. The space between the TE couple and plates of the channel are filled with insulators, where three different values of the thermal conductivities were investigated (k can be 0 for perfect insulation; 0.015 W/m-K and 0.05 W/m-K). The thermal conductivity k of the conducting copper plates was taken to be 387.36 W/m-K. The thermal conductivity of the TE material in W/m-K is given by[8]

$$k(T) = 0.23912+609.95/T-838.3/T^2 \qquad (1)$$

For this problem, there are a number of symmetry planes: one midway between the middle two plates and a symmetry plane midway between TE couples in the spanwise direction. Thus, the domain of the problem investigated is the one shown in Fig. 3.

Table 1 gives a summary of all cases simulated for TEPG 1. In this table, H is the half-height of the hot-gas passage, and V is the speed of the hot-gas flow at the hot-gas passage inlet. k_{plate} is the thermal conductivity of the plate. It was set to zero to model adiabatic wall and to 0.05 to model a wall that is as good as an insulator. $k_{insulator}$ is the thermal conductivity of the insulation material that fill the space between the TE couple and the channel plates. It was set to zero to model perfect insulation. Contact (no or yes) indicates with the aluminum

plate touches or does not touch the TE legs. Re_{2H} and Re_L denote the Reynolds number based on channel height (2H) or the total length of the channel (L). A flow in a circular pipe needs to have a Re_D (where D is diameter) greater than about 2,300 to achieve turbulent flow if the pipe is long enough (at least about 140D). For boundary-layer flow on a flat plate with non-turbulent free stream flow, the Reynolds number based on the distance from the leading edge of the plate must exceed about 5 x 10^5 before the flow can become turbulent. Thus, for the conditions considered in this study, the flow in the channel is laminar. Nevertheless, a few simulations were carried out assuming turbulent flow throughout the channel in which the flow that enters the channel, though still has a uniform profile, has a 2% turbulence intensity.

Table 1. Summary of Cases Simulated for TEPG 1.

Case	H (mm)	V (m/s)	k_{plate} (W/m-K)	$k_{insulator}$ (W/m-K)	Contact	Re_{2H}/Re_L	Laminar / Turbulent
1-1	10	10	0	0	No	3,812/21,450	Laminar
1-2	10	10	0.05	0.05	No	3,812/21,450	Laminar
1-3	10	10	202.4	0.05	No	3,812/21,450	Laminar
1-4	5	10	202.4	0.05	No	1,906/21,450	Laminar
1-5	2.5	10	202.4	0.05	No	953/21,450	Laminar
1-6	10	5	202.4	0.05	No	1,906/10,725	Laminar
1-7	10	2.5	202.4	0.05	No	953/5,363	Laminar
1-8	10	10	202.4	0.05	Yes	1,950/21,450	Laminar
1-9	10	10	202.4	0.05	No	1,950/21,450	Turbulent
1-10	10	5	202.4	0.05	No	1,950/10,725	Turbulent
1-11	10	2.5	202.4	0.05	No	953/5,363	Turbulent
1-12	10	10	202.4	0.015	No	3,812/21,450	Laminar
1-13	10	10	202.4	0.015	No	3,812/21,450	Turbulent

TEPG 2 (impinge jets) The TEPG problem shown in Fig. 4 involves a hot gas with uniform temperature T_h of 600 K and uniform velocity v along the x direction (v can be 10 m/s or 20 m/s) entering a converging channel, where the channel height is 30 mm at the inlet and 10 mm at the channel's end. The hot gas entering this channel is diverted through a series of square holes (2.5 mm x 2.5 mm x 5 mm) into a channel with height of 10 mm to create jets that impinge on the top of the TE legs. The back pressure at the exit of this channel is maintained at 1 atm. The plate with the square holes that separate the two channels has a thickness of 5 mm and is made of aluminum with thermal conductivity of 202.4 W/m-K. Each of the TE legs has a 5 x 5 mm^2 cross section, and its length can be 5 mm or 10 mm. The copper conducting plates that connect the TE legs have a thickness of 0.5 mm and have a thermal conductivity of 387.36 W/m-K. The thermal conductivity of the TE material is given by Eq. (1). The cold plate on the other side of the TE couple is maintained at 300 K. Similar to TEPG 1, TEPG 2 also has a number of symmetry planes: a symmetry plane midway between TE couples in the spanwise direction. Thus, the domain of the problem investigated is the one shown in Fig. 4.

Table 2. Summary of Cases Simulated for TEPG 2

Case	V (m/s)	h_{TE} (mm)
2-1	10	5
2-2	20	5
2-3	10	10
2-4	20	10

CHAPTER IV. Governing Equations and Method of Solution

The problems described in the previous section involve a gas whose density can change significantly from large changes in temperature even though the Mach number of the flow is quite low. Also, the flow can be laminar or turbulent depending upon the Reynolds number and conditions of the flow that enter the channels. In this study, when the flow is laminar, the governing equations used are the continuity, Navier-Stokes, and energy equations for an ideal gas. When the flow is turbulent, the governing equations used are the ensemble-averaged continuity, Navier-Stokes, and energy equations for an ideal gas. The effects of turbulence were modeled by the two-equation realizable k-ε model.[18] Wall functions were not used, and integration of all equations is to the wall, resolving the low-Reynolds number region of the turbulent boundary layers. In the near-wall region, the one-equation two-layer model of Chen and Patel[19] is used. This model divides the turbulent flow field into two regions. One region, referred to as the wall region, extends from the wall to the edge of the fully turbulent region. The other region, referred to as the core region, contains the rest of the turbulent flow field which is fully turbulent everywhere. In the wall region, the one-equation model of Wolfshtein[20] is used, and in the core region, the realizable k-ε model is used. For the solid phases – channel plates, electrical conducting plates, TE material, and insulation material – the Fourier law is used.

Solutions to the governing equations were obtained by using Version 6.3.26 of the Fluent-UNS code.[21] Only steady-state solutions were sought, and the fully coupled implicit algorithm was used to generate solutions, where momentum, continuity, and energy were

solved simultaneously instead of in a segregated fashion. All equations were integrated over each cell of the grid system. The fluxes for density, momentum, and energy at the cell faces are interpolated by using the third-order MUSCL scheme. Pressure was computed by using second-order accuracy. For all computations, iterations were continued until all residuals for all equations plateau to ensure convergence to steady-state has been reached. At convergence, the normalized residuals were always less than 10^{-12} for computations involving laminar flows. When the flow is turbulent, the normalized residual is always less than 10^{-5} for the three components of the velocity, less than 10^{-7} for the energy, less than 10^{-5} for turbulent kinetic energy, less than 10^{-4} for dissipation rate of turbulent kinetic energy, and less than 10^{-3} for the continuity equation.

The accuracy of CFD solutions is strongly dependent upon the quality of the grids used in minimizing grid-induced errors and in resolving the relevant flow physics. Figure 5 shows the grid used for TEPG 1, and Fig. 6 shows the grid used for TEPG 2. For TEPG 1, the grid sensitivity study involved two grids, one with 1,102,200 cells (referred to as baseline) and one with 1,815,528 (referred to as refined and the refinement was made in regions with the steepest gradients). From Fig. 7, it can be seen that the predicted temperature (a scalar quantity) and heat flux (a gradient) along on the hot surface (Y=0) is essentially the same for the two grids (maximum relative error is much less than about 0.01%). Thus, the baseline grid is used for all cases studied. For TEPG 2, the grid sensitivity study involved three grids, one with 1,284,120 cells (referred to as baseline), one with 968,224 cells for 5 mm tall TE legs and 985,296 for 100mm tall legs (referred to as coarser), and one with 1,929,464 (referred to as refiner). From Fig. 8, it can be seen that the predicted temperature along on

the hot surface (Y=0) is essentially the same for the baseline and the finer grids (maximum relative error is less than about 0.5%). Thus, the baseline grid is used for all cases studied. For both TEPG 1 and TEPG 2, y+ of the first grid point is less than unity for all Reynolds numbers studied.

Top view ➡

⬆ Front view   ⬆ Side view
- Grid number: 1,102,200
- Insulator is not shown in left figures
- All grids are structure mesh

baseline ➡

refined ➡

- Grid number: 1,815,528
- Insulator is not shown in left figures.
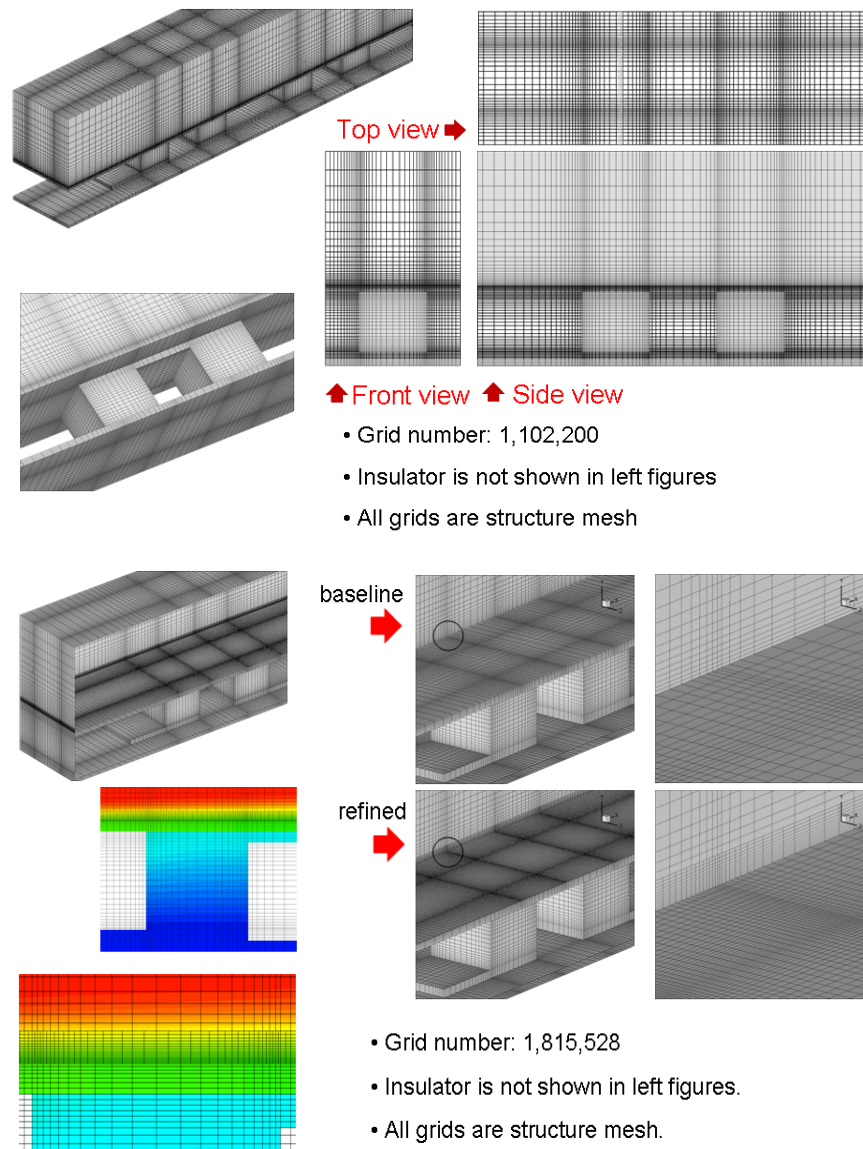- All grids are structure mesh.

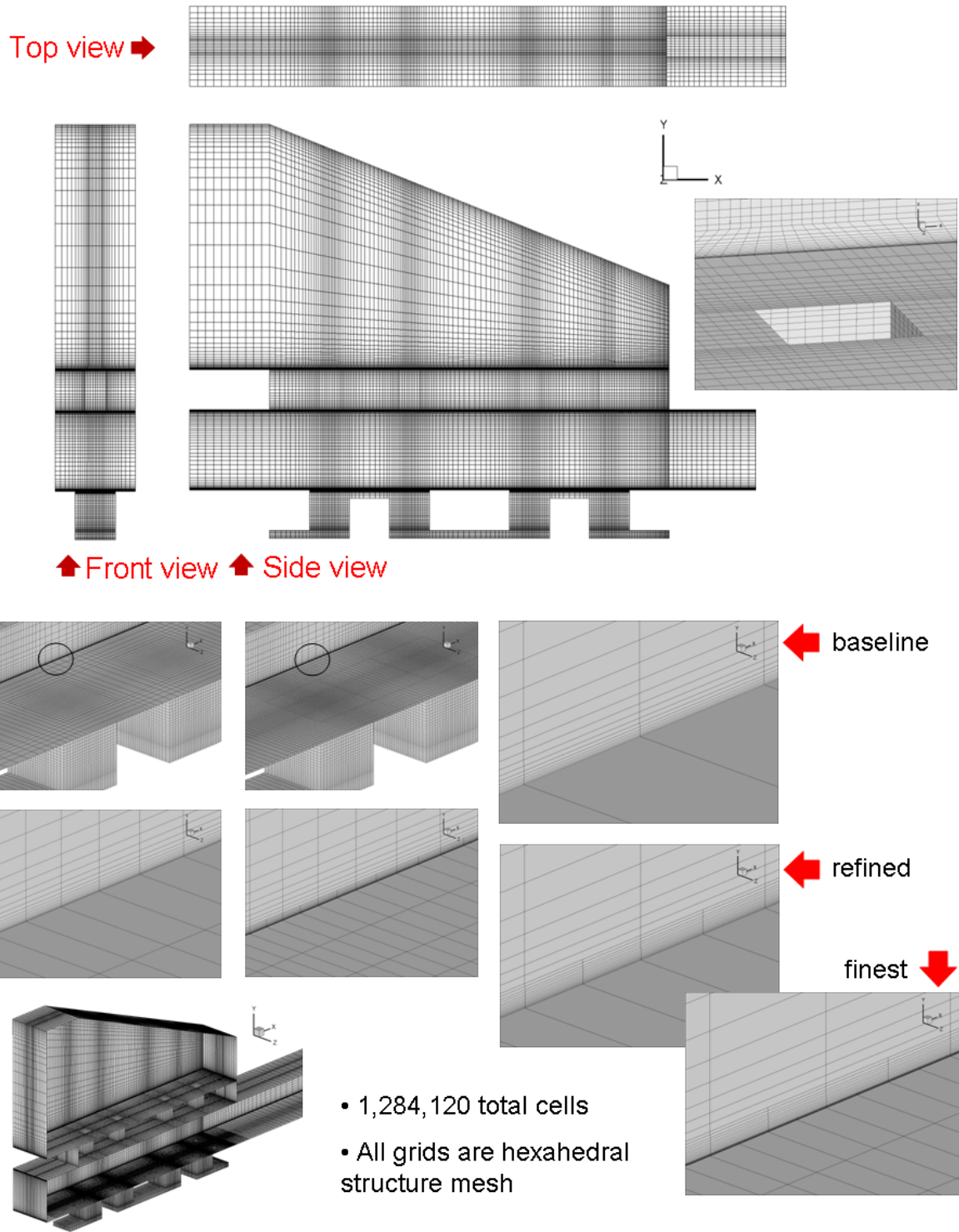Fig. 5. Grid system used for TEPG 1.
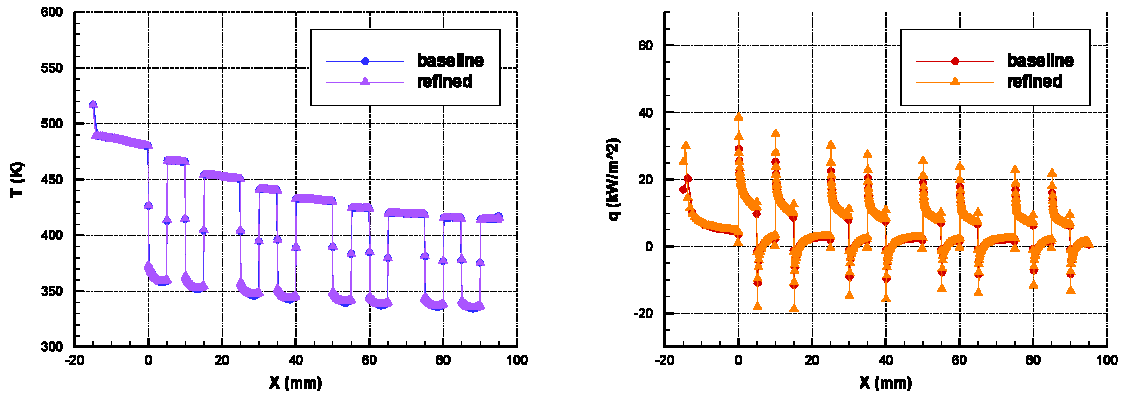
Fig. 6. Grid system used for TEPG 2.

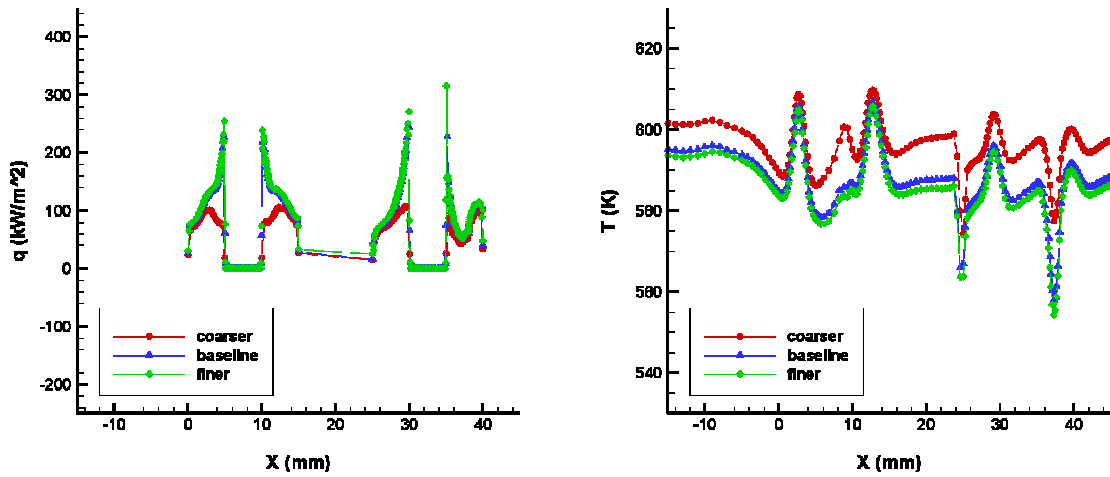Fig. 7. Grid sensitivity study for the TEPG 1 problem.

Fig. 8. Grid sensitivity study for the TEPG 2 problem.

CHAPTER V. Results

CFD analyses were performed to examine two TEPGs with focus on the flow and heat-transfer processes about the TE couples. The CFD simulations performed are summarized in Tables 1 and 2. In this section, the results generated are presented.

5.1 TEPG 1

The results generated for TEGP 1 are summarized in Table 3 and Figs. 9 to 15.

5.1.1 Effects of Thermal Conductivity

Cases 1-1 to 1-3 in Table 1 examine the effects of thermal conductivity of the HX channel plates and the insulation material. This is of interest because the thermal conductivity of the TE material is quite small, around 1 to 2 W/m-K (see Eq. (1)) so that the conduction resistance in the metals such as in the aluminum plates of the HX channel and the copper conducting plates of the TE couple are negligible in comparison to the conduction resistance in the TE legs and the insulation material.

Table 3. Results for TEPG 1.

Units: q in W, q″ in W/cm^2

Case	$q_h / q_h^{''}$	$q_{cold} / q_{cold}^{''}$	$q_p / q_p^{''}$	$q_c / q_c^{''}$	$q_i / q_i^{''}$	Average ΔP (Pascal)
1-1	3.04/1.52	3.04/1.52	0	0	0	10.847
1-2	2.54/1.27	3.88/1.94	0	0.19/0.96	1.15/0.053	10.198
1-3	2.28/1.14	4.52/2.26	0	0.37/1.85	1.86/0.087	9.889
1-4	2.37/1.18	4.63/2.31	0	0.37/1.86	1.89/0.088	19.832
1-5	2.55/1.27	4.85/2.42	0	0.38/1.89	1.92/0.090	42.836
1-6	1.66/0.83	3.62/1.81	0	0.33/1.65	1.63/0.076	3.249
1-7	1.21/0.60	2.88/1.44	0	0.28/1.42	1.38/0.065	1.125
1-8	1.24/0.62	6.16/3.08	4.66/5.82	-0.06/-0.32	0.33/0.015	9.329
1-9	2.69/1.34	5.15/2.57	0	0.40/2.02	2.06/0.096	10.276
1-10	1.75/0.88	3.79/1.89	0	0.34/1.71	1.69/0.079	3.211
1-11	1.21/0.61	2.89/1.45	0	0.29/1.43	1.39/0.065	1.096
1-12	2.84/1.42	3.90/1.95	0	0.19/0.96	0.87/0.041	10.351
1-13	3.26/1.63	4.40/2.20	0	0.20/1.02	0.94/0.044	10.677

ΔP = inlet stagnation pressure – outflow stagnation pressure
q = average heat transfer rate over 8 TE legs (W)
q″ = average heat flux over 8 TE legs (W/cm^2)
Subscripts for q and q″ denote:
    h = heat transfer rate into TE leg from hot gas
    cold = heat transfer rate TE leg's cold side
    p = heat transfer rate into TE leg from the hot plate
    c = heat transfer rate into TE leg from the conductor
    i = heat transfer rate into TE leg from the insulator to the conductor

Case 1-1 has perfect insulation since k_{plate} = $k_{insulation}$ = 0. For this case, all thermal energy from the hot gas can only be transferred through the TE couple, which represents an ideal case in capturing all thermal energy from the hot gas for electrical energy conversion. Case 1-2 represents a situation closest to the ideal case since the thermal conductivity of the channel plate is made equal to that of the insulation material (i.e., k_{plate} = $k_{insulation}$ = 0.05 W/m-K). Case 1-3 has the correct thermal conductivities for the aluminum plates and the

insulation material. From Table 3, it can be seen that the heat transfer from the hot gas to the

TE leg (q_h and $q_h{''}$) at Y=0 is indeed the highest for Case 1-1 with heat flux at 1.52 W/cm^2,

lower for Case 1-2 at 1.27 W/cm^2, and lowest for Case 1-3 at 1.14 W/cm^2. However, when

there is conduction through the channel plate and the insulation material, some of the thermal

energy is still transferred to the TE legs since the thermal conductivity of the TE material

though low is still higher than the thermal conductivity of the insulation material. Table 3

shows that only for Case 1-1 with perfect insulation (i.e., $k_{plate} = k_{insulation} = 0$) does q_h (and

$q_h{''}$) equal to q_{cold} (and $q_{cold}{''}$) (i.e., the heat transfer from the hot gas to the TE leg at Y=0

equals to the heat transfer from the TE leg to the cold plate at Y=-h). For Case 1-2, $q_{cold}{''}$ is

1.94 W/cm^2, and for Case 1-3, it is 2.26 W/cm^2. On this, it is noted that when there is heat

transfer from the hot gas to the channel plates and the insulation material, a portion of that

thermal energy is then transferred to the electrical conducting plates of the TE couple, which

in turn are transferred to the TE leg. For Case 1-2, that heat flux $q_c{''}$ is 0.96 W/cm^2, and for

Case 1-3, it is 1.85 W/cm^2. The heat flux $q_i{''}$ from the insulation material to the TE leg is

0.053 W/cm^2 for Case 1-2 and 0.087 W/cm^2 for Case 1-3. Whether higher heat-transfer rate

through a portion of the TE leg leads to higher electric-current flow through the entire TE

couple is unclear. Nevertheless, one would expect shape optimization of the TE legs to offer

opportunities for improved conversion efficiency.

Figure 9 shows the temperature on the surface of the channel plate and the TE legs exposed

to the hot gas at Y=0 and in the mid-plane through the center of TE couples at Z=0 for Cases

1-1 and 1-3. When the insulation is perfect as in Case 1-1, the surface temperature at Y=0 is

essentially equal to the hot-gas inlet temperature T_h (600 K) everywhere except along a path

over the TE legs and the thermal boundary layers that develop from there. It is important to note that the heat transfer through the TE legs is not one-dimensional even for Case 1-1 because the temperature over each TE leg at Y=0 decreases with X because of the growth of the thermal boundary layer. When the insulation is imperfect as in Case 1-3, the surface temperature at Y=0 is considerably lower than that for Case 1-1. However, because the thermal conductivity of the plate is much higher than that of the TE material and the insulator, it can be seen from Fig. 9 that the entire channel plate is at nearly the same temperature. The temperature in the TE legs, however, is still not one dimensional because the gas temperature in contact with the TE material changes along X. Also, there is heat transfer into the TE leg from the conducting plates and the insulation material.
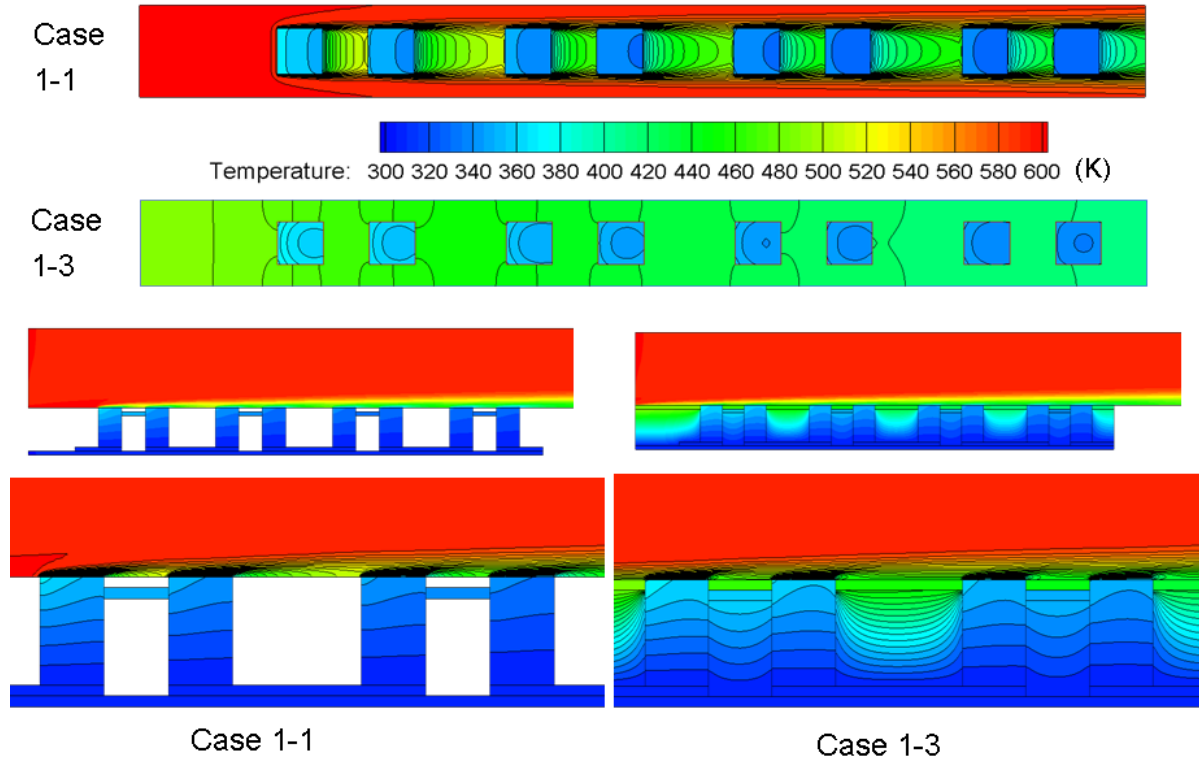

Fig. 9. Temperature contours in two planes: Y=0 and Z=0 for Cases 1-1 and 1-3.

Figure 10 shows the temperature and the X-component velocity contours in several Y planes next to the channel wall exposed to the hot gas for Case 1-3, and Fig. 11 shows the temperature and X-component velocity profile at Z=0 and several X locations about the TE legs. From Fig. 11, it can be seen that the heat transfer into the TE legs reduces the temperature of the gas about the TE leg and, while doing so, increases the gas' X-component velocity. The increased X-component velocity is a result of increased density next to the wall because of the lower temperature there, which accelerated flow further away from the wall towards the wall.
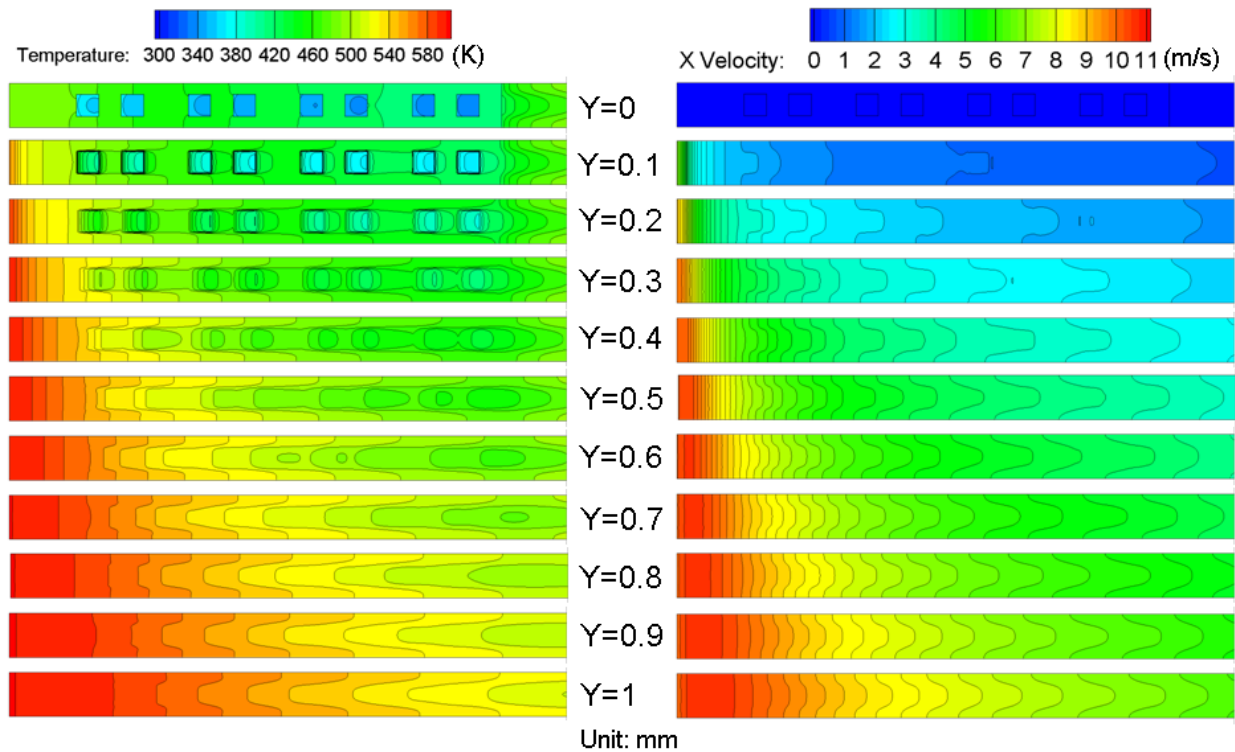

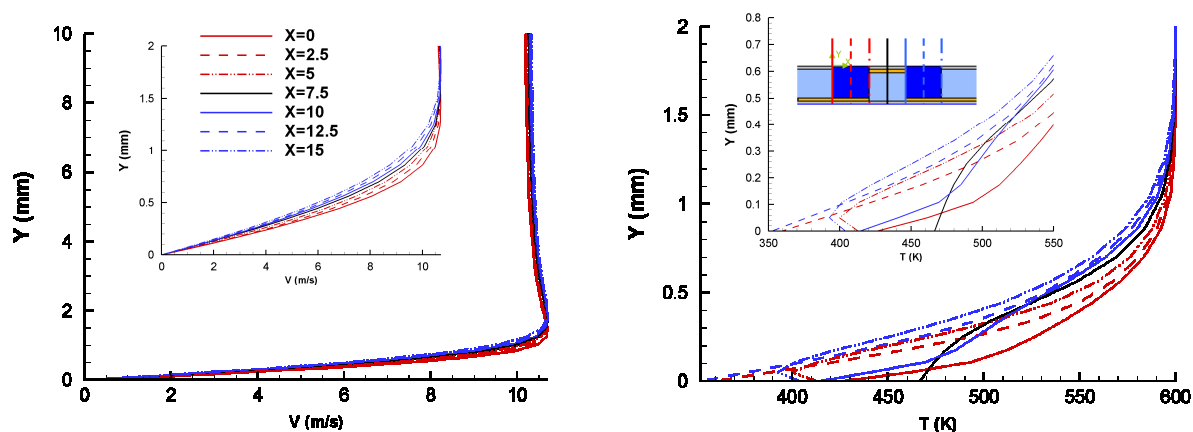Fig. 10. Temperature and X-component velocity in several Y planes for Case 1-3.

Fig. 11. Profile of temperature and X-component velocity at Z=0 and selected X locations
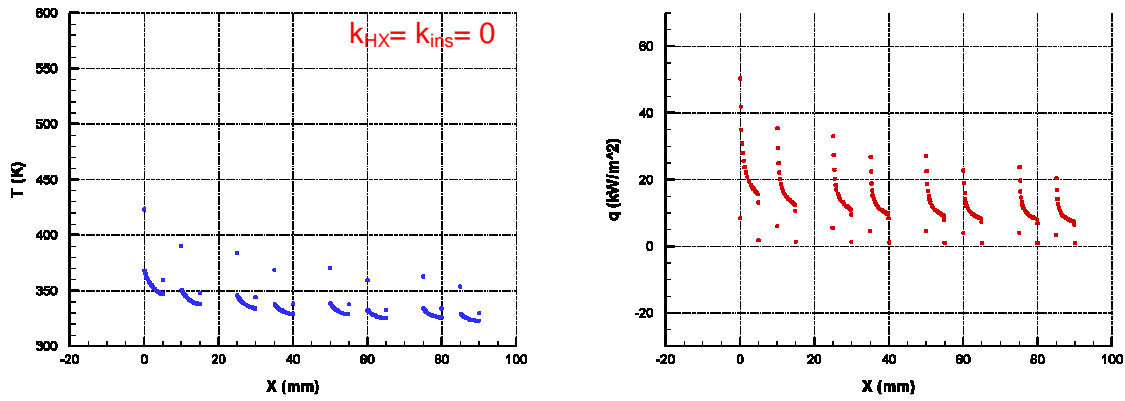
for Case 1-3.

Near the wall at Z = 0, Fig. 11 shows the peak velocity to be higher than the inlet velocity by

almost 1 m/s, which is much higher than possible from the increased displacement thickness.

Figure 11 also shows the temperature along X to reduce when in contact with the TE legs and

to increase when in contact with the plate. This is because the entire plate with high thermal

conductivity is heated to nearly uniform temperature by the hot gas and serves as a storage

device that transfers heat to the hot gas when it is colder than the plate. Figure 12 shows the

temperature along the line on the middle of the wall next to the hot gas at Y=Z=0. From

there, it can be seen that the temperature at the top of the TE leg (i.e., at Y=0) is highest for

Case 1-3, which has realistic values of thermal conductivity, and lowest for Case 1-1, which

has perfect insulation. The temperature on top of the TE legs is higher for Cases 1-2 and 1-3

than for Case 1-1 because heat is being transferred there through the channel plate and the

electrical conducting plates. Though the temperature on top of the TE leg is the lowest for

Case 1-1 and highest for Case 1-3, the heat flux at top of the TE leg is highest for Case 1-1

and lowest for Case 1-3. This is because Case 1-1 does have the thinnest thermal boundary layer.

Figure 12 also shows that for Case 1-3, the heat flux at Y=0 can be positive and negative. Basically, the heat transfer can be from the hot gas into the TE legs and from the channel wall to the hot gas. This phenomena is also observed for all the Cases involving TEPG1 except Cases 1-1, 1-2, and 1-8. This is because when the hot gas flows in, the aluminum plate was heated up at the entrance region. As noted earlier, the channel wall with its high thermal conductivity is heated up quickly and to nearly uniform temperature because the thermal conductivities of the TE legs and insulation material are so low. Thus, it is possible for the hot gas to get cooler than the channel plate because of heat transfer to the TE legs.

Since pressure loss should be kept to the minimum for efficiency, the stagnation pressure from the channel inlet to the channel outlet is monitored. For Cases 1-1 to 1-3, the pressure loss is highest for Case 1-1 and lowest for Case 1-3 (Table 2). This is because the viscosity is lower at lower temperatures.
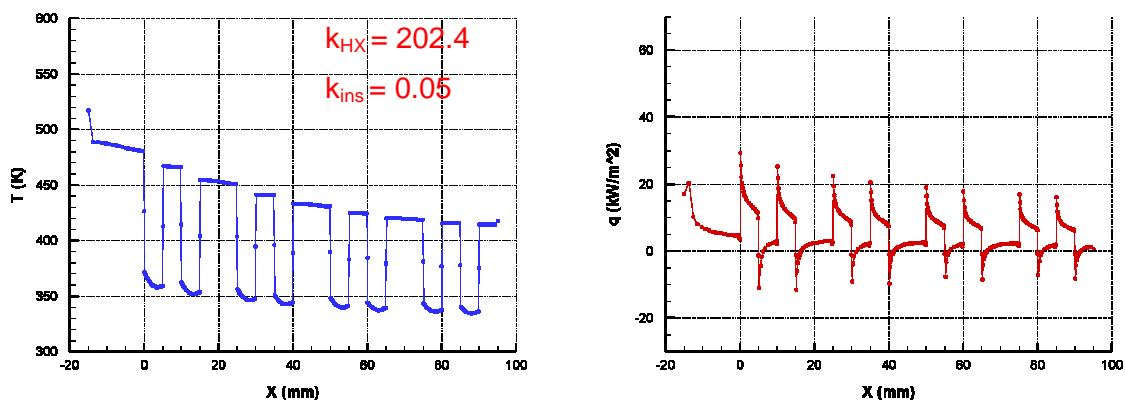
23
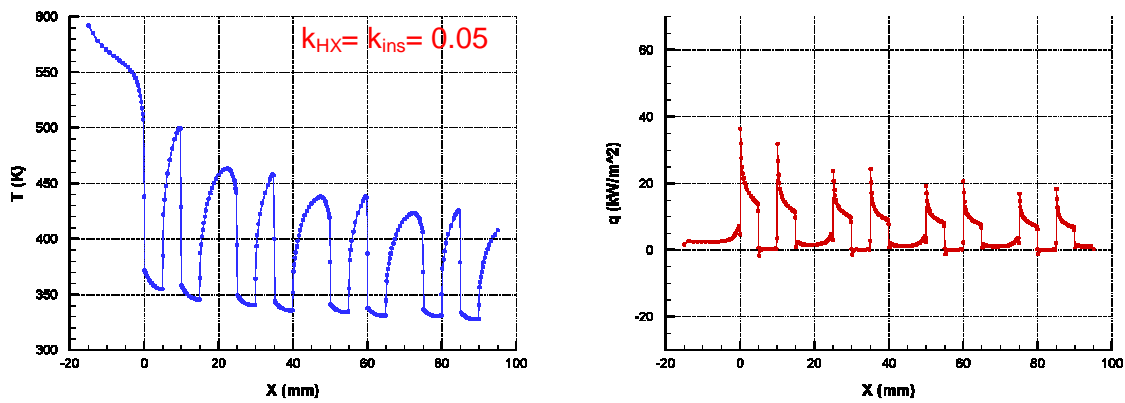
Case 1-1

Case 1-2

Case 1-3

Fig. 12. Temperature and heat flux along X at Y=Z=0 for Cases 1-1, 1-2, and 1-3.

5.1.2 Effects of Hot-Gas Channel Height, Inlet Velocity, Reynolds Number, and Turbulence

Cases 1-3, 1-4, and 1-5 examine effects of H to see how small H can be and still have boundary layers from the two opposite walls of the channel not interact significantly in terms of heat transfer. From Fig. 13, it can be seen even with H of 2.5 mm (or a channel height of 5 mm), the heat transfer to the top of the TE leg does not change appreciably. The slight increase in heat transfer as H decreases is due to the increase in the core speed from growth of the displacement thickness. The pressure drop, however, does increase appreciably as H decreases to 2.5 mm as shown in Table 3 and Fig. 15 because of increased shear stress. Since the boundary layers from the two walls of the hot-gas passage do not interact, the Reynolds number based on 2H is not meaningful.

Cases 1-3, 1-6, & 1-7 examine the effects of the inlet velocity. For a given channel height, as the inlet velocity decreased, the thickness of momentum and thermal boundary layers increased. As a result, heat transfer decreased as shown in Table 3 and Fig. 13.

Cases 1-3 and 1-8 examine the effect of the fit when the TE legs of the TE couples are inserted in square holes of the channel plate that come in contact with the hot gases. For Case 1-3, the TE legs do not touch the walls of the square holes so that the channel plate cannot transfer heat to the TE legs. For Case 1-8, the TE legs do touch the walls of the walls of the square hole with a tight fit from thermal expansion. Figure 13 and Table 3 show that by having contact, the heat transfer to the TE legs from the hot gas at Y=0 decreases though

the overall heat transfer through the TE legs increases. The decrease in heat transfer from the hot gas at Y=0 results because the TE leg is heated by the plate.

Cases 1-3, 1-6, 1-7, 1-9, 1-10, and 1-11 examine the effects of laminar versus turbulent flow in the hot-gas passage. From Fig. 14 and Table 3, it can be seen with turbulent flow, the heat transfer does increase somewhat, but not appreciably except at higher inlet velocities.

Cases 1-12 and Case 1-13 were simulated to examine the effects of improved insulation material with thermal conductivity of 0.015 W/m-K. With improved insulation, heat transfer to the TE leg increases as expected.

For TEPG1, the change in the thermal energy from inlet to outlet due to heat transfer to the TE couples ranges from 1.2~2.7 % when H = 10mm. It can be as high as 5.7 % when H = 2.5mm. Thus, only a very small fraction of the thermal energy in the hot gas has been extracted. To extract more energy requires H to be made smaller. With a smaller H, the pressure drop is higher. Thus, need to find the optimum H.
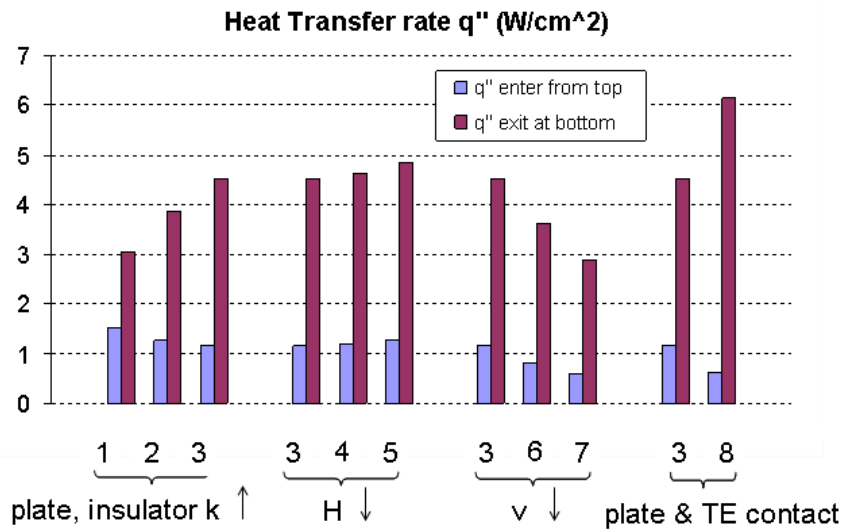
Heat Transfer rate q" (W/cm^2)

Fig. 13. Average heat flux from hot gas into TE leg at Y=0 (blue) and from TE leg to cold wall at Y=-h (red). 1, 2, …, 8 denote Cases 1-1, 1-2,…, 1-8.

Heat Transfer rate q" (W/cm^2)

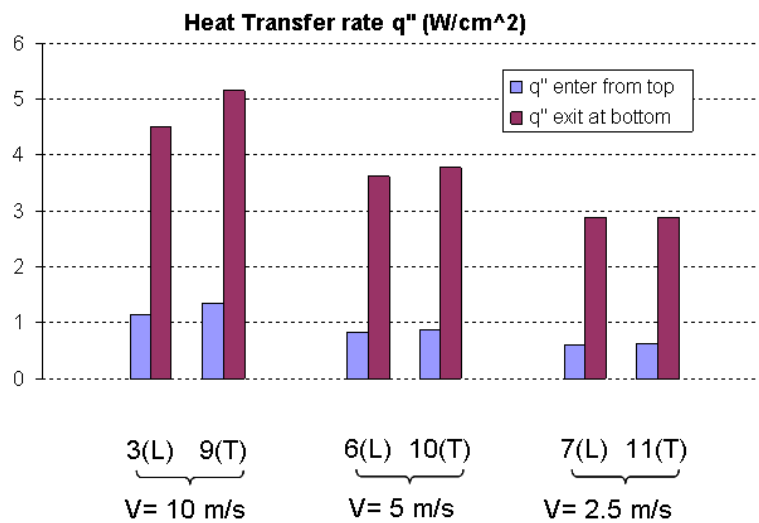Fig. 14. Average heat flux from hot gas into TE leg at Y=0 (blue) and from TE leg to cold wall at Y=-h (red). 3, 9, …denote Cases 1-3, 1-9,…. L denotes laminar & T denotes turbulent.
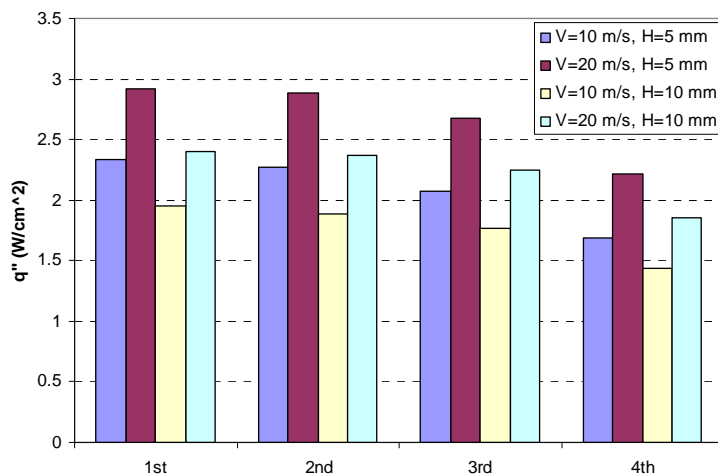

Fig. 15. Average heat flux from hot gas into TE leg at Y=0 (blue) and pressure drop across HX. 1, 2, … denote Cases 1-1, 1-2, …..

5.2 TEPG 2

The results generated for TEGP 2 are given in Figs. 16 to 18. Figure 16 shows the temperature distribution on the surface at Y=0 where hot-gas jets impinges and at a mid-plane at Z=0 that passes through the middle of the TE couples. Also shown in this figure are the temperature and heat flux at Y=Z=0. From this figure, it can be seen that with an inlet velocity of 10 m/s, the jets created through the square holes are deflected quite a bit by the cross flow. With an inlet velocity of 20 m/s, the deflection of the jet by the cross flow is less. Also, the temperature of the surface struck by the jet is hotter so that the heat flux is also higher. Figure 17 shows the projected streamlines in several constant Z planes. From this figure, it can be seen that the flow induced by the jets is quite complicated. Understanding these jets and their deflection by the cross flow is needed to ensure that the hot-gas jets impinge on top of each of the TE legs of the TE couples. For the conditions of the present study, Fig. 18 shows that the heat flux can be as high as nearly 3 W/cm^2. The pressure drop from inlet to outlet, however, is considerable higher than that of TEPG 1. It is about 8,000 Pa when the inlet velocity is 10 m/s and 38,000 Pa when the inlet velocity is 20 m/s.

From the 4 cases studied, the heat removed from the 4 TE legs is about 1 % of the thermal energy at the inlet when V = 20 m/s and 1.3~1.5 % when V = 10 m/s. Though more heat is transferred to the TE legs when V is higher, the fraction of the energy extracted is less.
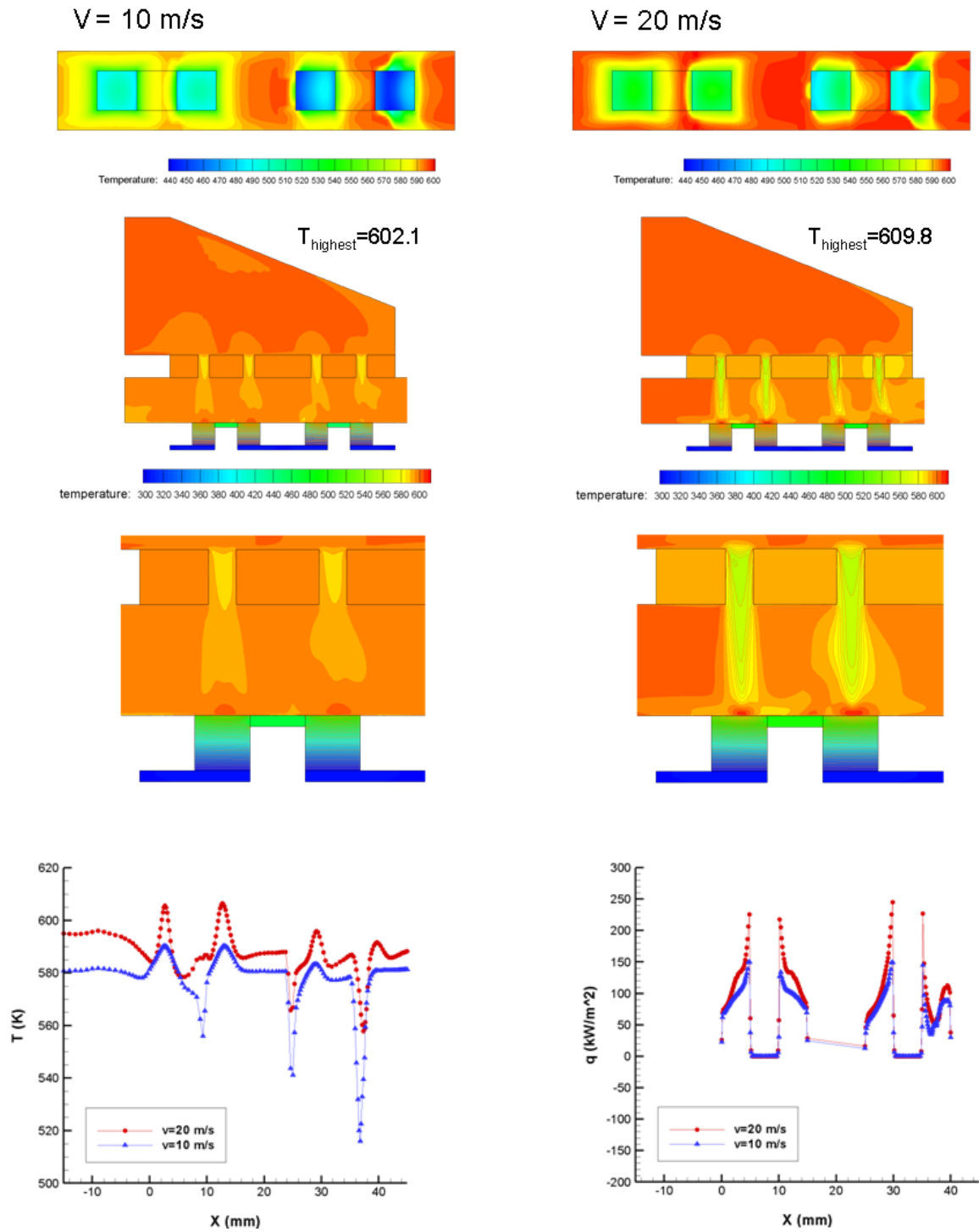
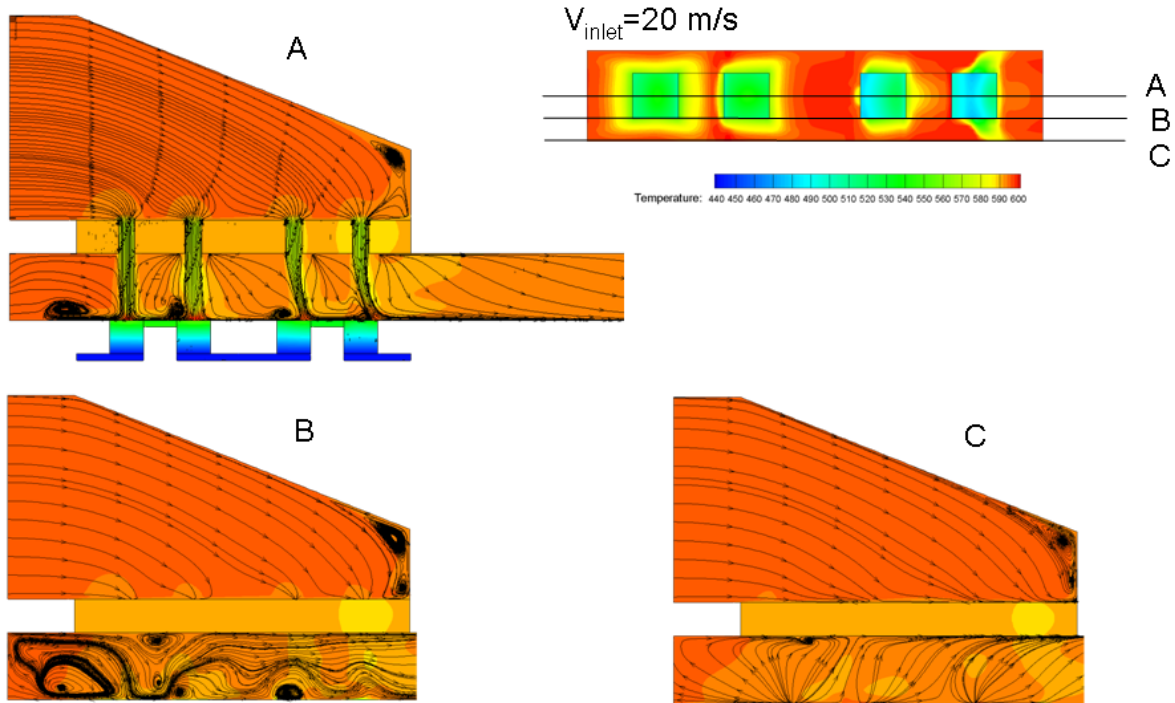Fig. 16. Temperature distribution at Y=0 and at Z=0 and temperature and heat flux at

Y=Z=0.

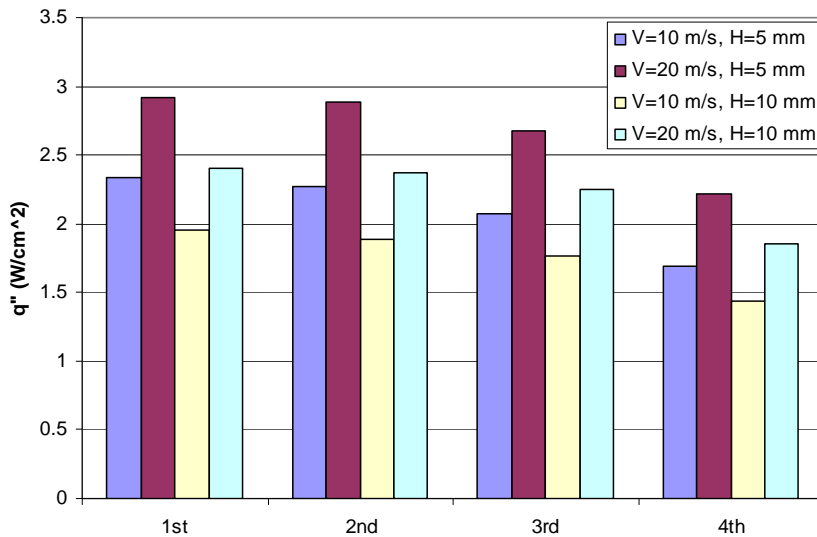Fig. 17. Temperature distribution at Y=0 and three Z planes with projected streamlines.

Fig. 18. Average heat flux from hot gas into TE leg at Y=0/ 1st, 2nd, … denote the first,

second, … TE legs.

CHAPTER VI. Summary

CFD analyses were performed to examine two TEPGs with focus on the flow and heat-transfer processes about the TE couples. When the heat-transfer enhancement in the TEPG is based on the leading portion of developing boundary layers, the heat transfer to the TE material can be as high as 1 W/cm^2 with reasonable pressure drop. When the heat-transfer enhancement is via jet impingement, the heat transfer to the TE material can be as high as 3 W/cm^2 but with markedly higher pressure drop. Results obtained also show the heat-transfer process through the TE legs to be multidimensional with heat entering from the top of the TE legs exposed to the hot gas and from the insulators and the conducting plates.

REFERECE

1. Rowe, D. M., Editor, *CRC Handbook of Thermoelectrics*, CRC Press, Boca Raton, 1995.

2. Rowe, D.M., Editor, *Thermoelectric Handbook: Macro to Nano-Structured Materials*, Taylor and Francis Books, 2005.

3. Majumdar, A., "Microscale Heat Conduction in Dielectric Thin Films," *ASME Journal of Heat Transfer*, Vol. 115, pp.7-16, 1993.

4. Chen, G., "Size and Interface Effects on Thermal Conductivity of Superlattices and Periodic Thin-Film Structures," *ASME Journal of Heat Transfer*, Vol. 119, pp. 220-229, 1997.

5. Chen, G., "Ballistic-Diffusive Heat Conduction Equations," *Physics Review Letters*, Vol.86, pp 2297-2300, 2001.

6. Bhandari, C.M., "Size Effects on Thermal Transport," in *Thermoelectric Handbook: Macro to Nano-Structured Materials*, Editor: Rowe, D.M., Taylor and Francis Books, 2005, Chapter 14.

7. Stevens, J.W., "Optimized Thermal Design of Small ΔT Thermoelectric Generators," *Proeedings of the 34th Intersociety Energy Conversion Engineering Conference*, Vancouver, British Columbia, Aug. 1999.

8. Hogan, T. and Shih, T.I-P., "Modeling and Characterization of Power Generation Modules Based on Bulk Materials," *Thermoelectric Handbook: Macro to Nano-Structured Materials*, Editor: M. Rowe, Taylor and Francis Books, 2005.

9. Harris, R., Schock, H.J., and Hogan, T., and Shih, T., "Heat Transfer and Electric Current Flow in a Thermoelectric Couple," AIAA Paper 2006-0575, Aerospace Sciences Meeting, Reno, Nevada, January 2006.

10. Zhu, B., Schock, H.J., Hogan, T., and Shih, T. I-P., "Natural Convection and Radiation Heat Transfer in High-Temperature Thermoelectric Couples," AIAA Paper 2006-0574, Aerospace Sciences Meeting, Reno, Nevada, January 2006.

11. Han, J.C., Dutta, S., and Ekkad, S.V., *Gas Turbine Heat Transfer and Cooling Technology*, Taylor & Francis, New York, 2000.

12. Sundén, B. and Faghri, M., Editors, *Heat Transfer in Gas Turbines*, WIT Press, Ashurst, Southhampton, 2001.

13. Shih, T.I-P. and Sultanian, B., "Computations of Internal and Film Cooling," *Heat Transfer in Gas Turbines*, Editors: B. Sundén and M. Faghri, WIT Press, Ashurst, Southhampton, 2001, Chapter 5, pp. 175-225.

14. Gardon, R, and Carbonpue,J., "Heat Transfer between a Flat Plate and Jets of Air Impinging on It," *International Developments in Heat Transfer*, Vol. 2, 1962, pp. 454-460.

15. Martin, H., "Heat and Mass Transfer between Impinging Jets", *Advances in Heat Transfer*, Vol. 13, 1977, pp. 1-60.

16. Narayanan, V., Sayed-Yagoobi, J. and Page, R.H., "An experimental Study of Fluid Mechanics and Heat Transfer in an Impinging Slot Jet Flow", *Int. Journal of Heat and Mass Transfer*, Vol. 47, 2004, pp. 1827-1845.

17. Garimella, S. V. and Schroeder, V. P., 2001, "Local Heat Transfer Distributions in Confined Multiple Air Jet Impingement", *Journal of Electronic Packaging*, Vol. 123, pp. 165-172.

18. Shih, T.-H., Liou, W., Shabbir, A., and Zhu, J., "A New k-ε Eddy-Viscosity Model for High Reynolds Number Turbulent Flows – Model Development and Validation," *Computers and Fluids*, Vol. 24, No. 3, 1995, pp. 227-238.

19. Chen, H.C. and Patel, V.C., "Near-Wall Turbu-lence Models for Complex Flows including Separation," *AIAA Journal*, Vol. 26, No. 6, 1988, pp. 641-648.

20. Wolfshtein, M., "The Velocity and Temperature Distribution in One-Dimensional Flow with Turbulence Augmentation and Pressure Gradient," *International Journal of Heat and Mass Transfer*, Vol. 12, 1969, pp. 301-318.

21. Fluent license provided by ANSYS,
URL: http://www.fluent.com/software/fluent/index.htm.